A Comparative Study between FGM and SLF Approach for Turbulent Piloted Flame of Methane

MOKHTARI BOUNOUAR, GUESSAB AHMED
Department of Mechanical Engineering,
National Polytechnic School of Oran (Maurice Audin),
Postbox 1523 EL-M'naouer, Es-Senia Oran,
ALGERIA

Abstract: - This study validates the RANS simulation results by comparing them with experimental data. Numerical simulations were performed for a piloted methane-air jet flame in an axisymmetric burner. It is noteworthy that RANS simulations have been performed using a Non-premixed model with Steady Laminar Flamelet (SLF) and a partially premixed model with Flamelet Generated Manifold (FGM) of the Ansys-Fluent solver are used to express the chemistry-turbulence interaction, to provide an initial solution to the simulation performed by the Pdf transported, joint two kinetic mechanisms for oxidation of methane, detailed GRI-Mech 3.0 mechanism (53 species, 325 reactions), and CH_4-Skeletal mechanism (16 species, 41-step). The case test consists of a rich premixed flame (Sandia Flame D). A comparison between the results of the obtained simulations and experimental data shows good agreement, in particular in the context of RANS/FGM with both mechanisms (GRI 3.0 and CH_4-Skel).

Key-Words: - RANS, Flamelet, FGM, CH_4-Skeletal, GRI-Mech 3.0, Flame D, Methane.

Received: January 16, 2023. Revised: November 21, 2023. Accepted: December 17, 2023. Published: December 31, 2023.

1 Introduction

Numerical modeling is an extremely important tool for properly studying reactive turbulent flows. He probably has some preferences (gain time, less expensive than the experience, etc.). Skeletal mechanisms, specific to a particular type of problem, oxidation, and/or a certain range of conditions, are often derived from detailed mechanisms. Among the mechanisms published in the literature, the basic description of methane oxidation includes several dozen to a hundred reactions among 10 to 40 species. To obtain a skeletal mechanism, eliminate species and reactions that are not relevant to the problem being considered. The detailed description of the skeletal mechanism (CH_4-Skel) has been successfully used, [1], [2], [3], [4], [5], [6]. The CH_4 oxidation mechanism is the basis of the detailed mechanisms for natural gas and other hydrocarbons. This is the latest available version of GRI-Mech 3.0, [7].

As for the previous versions, this mechanism was first developed for natural gas. The mechanism incorporates the oxidation kinetics of N_2.

Note that the FGM [8] and SLF [9], models are fundamentally different from the steady laminar flamelet (SLF) model. For example, in the SLF model, the laminar flamelet is parameterized by strain, so that as the strain rate decreases toward the exit of the combustion chamber, the thermochemistry always strives for chemical equilibrium. In contrast, the FGM and SLF models are parameterized by the progression of the reaction, and the flame can be completely extinguished by adding dilution air, for example. To properly study the effect of the two combustion models with different reaction mechanisms for the oxidation of methane in the air, we chose the configuration of a controlled diffusion flame for our test case (Sandia Flame D). These flames are often used to stabilize the combustion process under harsh conditions, such as in gas turbine engines.

Piloted methane-air turbulent jet diffusion flames, namely, flames D, are numerically studied, [10], [11], [12], [13]. This flame has been experimentally recorded, [14]. This configuration creates a simple parabolic flow and uses a series of premixed flame heat sources to stabilize the main jet at the burner exit face. A 41-step skeletal mechanism of CH_4-Skel, and the GRI 3.0 detailed mechanism which involves 53 species are used in this simulation.

The goal of this work is to provide a compact skeletal and detailed kinetic mechanism for methane oxidation, which can be applied to combustion models: Nom-premixed and partially premixed.

2 Problem Description and Numerical Modeling

The geometry of this test is a cylindrical combustion chamber with coaxial injectors, methane is injected through the inner tube, and a pilot jet is injected through the outer tube, as shown in Figure 1.

The composition of the main jet is a mixture of methane and air, with a molar volume fraction of 25% CH_4 and 75% air. For the fuel flow, the uniform inlet gas velocity is 49.6 m/s at a temperature of 294 K. The pilot jet is a combustion product with a temperature of 1880 K and a uniform inlet gas velocity of 11.4 m/s. The pilot jet operates at an equivalence ratio of 0.77. Air flows parallel to the main jet with a speed of 0.9 m /s. Detailed test conditions for establishing limits and fuel, pilot jet, and air compositions are shown in Table 1.

Chemical models are used to determine the source terms of transport equations for chemical species. Although the CFD code integrates several combustion models, only non-premixed and partially premixed models with chemical kinetics are used in this study (FGM and SLF).

The chemical mechanism used in this comparison is the detailed kinetic mechanism of GRI-Mech 3.0, which represents the most comprehensive and standardized set of mechanisms for methane combustion. This mechanism includes 53 species and 325 reactions.

The reaction mechanism of CH_4-Skel includes 16 species (H_2O, CO_2, O_2, CH_4, CO, H, H_2, OH, O, CH_3, HCO, HO_2, H_2O_2, CH_2O, CH_3O, and N_2) and 41 reactions.

Figure 2 shows the computational domain of the Sandia Flame D RANS simulation. The grid is composed of 80×88 a node assuming axial symmetry and the grid is subdivided at the nozzle exit. The equations to be solved are the equation of motion for the average velocity component, the transport equation for the average mixing fraction and its dispersion, and the transport equation for the turbulent kinetic energy and its dissipation.

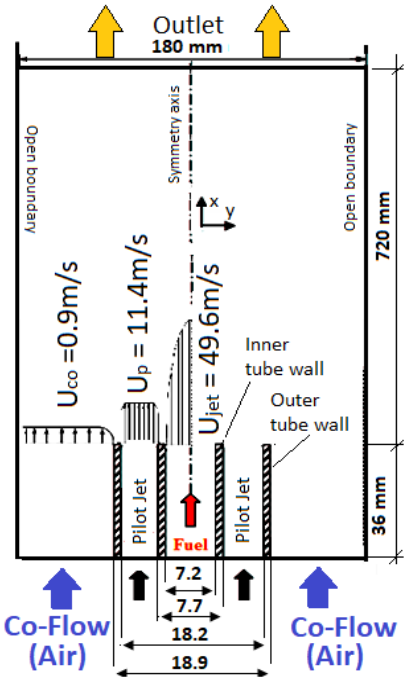

Fig.1: Burner configuration (All sizes are in mm)

Table 1. Condition for SANDIA Flame D [14].

		Main jet	Air Co-flow	Pilot Jet
Temperature [K]		294	291	1880
Velocity [m/s]		49.6	0.9	11.4
Composition (%)	Y_{CH4}	25	0	0
	Y_{O2}	15.75	21	0
	Y_{N2}	59.25	79	0
Mixture fraction, *f*		1	0	0.2755
Reaction progress variable, *c*		0	0	1
Turbulence intensity *I* [%]		10		10
Hydraulic diameter		72mm	/	16.5mm
Re		22400	/	/

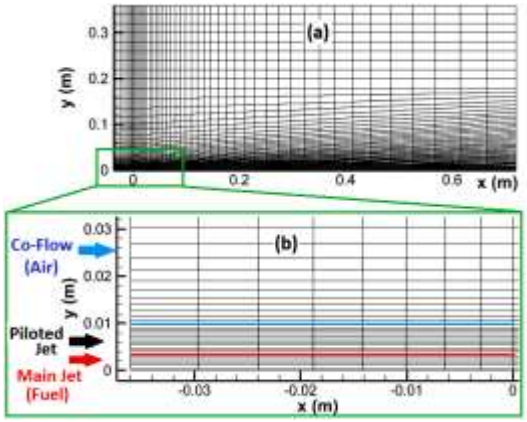

Fig. 2: (a) The computational mesh, (b) The detailed mesh

3 Flamelet Generated Manifold and Steady Laminar Flamelet

3.1 Flamelet Generated Manifold

Flamelet Generated Manifold (FGM) is a technology that chemically reduces combustion, [8], [9]. The method is based on the idea that the most important aspects of the internal structure of the flame front should be considered, and is based on a flamelet approach that reduces the number of equations to be solved and reduces CPU time. The FGM model provides the ability to solve transport equations for the variance of reaction progress variables or use algebraic expressions. In front of the flame, the fuel and oxidizer are mixed but do not burn, and behind the flame, the mixture burns.

The FGM model assumes that the scalar expansion of a turbulent flame can be approximated by the scalar expansion of a laminar flame. Diffusion FGM is computed using a laminar diffusion flamelet generator, as described in Flamelet Generation. A stable diffusion flame is created over a range of scalar dissipation rates by starting with a very small stretch (0.01/s by default) and gradually expanding (5/s by default) until the flame is extinguished. Diffusion FGM is computed from laminar flamelets with steady-state diffusion by converting the flamelet species field into reaction progress. The partially premixed combustion model with the FGM chemistry approach solves the transport equation for the average reaction progress variable *c*, the average mixture fraction f, and the mixture fraction variance, $f^{"2}$.

In front of the flame (c = 0) the fuel and oxidizer are mixed but do not burn, and behind the flame (c = 1) the mixture burns. A density-weighted average scalar (such as species proportion or temperature), denoted by $\bar{\phi}$, is computed from the probability density functions (PDFs) of f and c as follows:

$$\bar{\phi} = \int_0^1 \int_0^1 \phi(f,c) P(f,c) df.dc \qquad (1)$$

In addition to solving the RANS equation, the FGM model requires solving the following transport equations for *f, f"2*, and *c*:

$$\frac{\partial(\rho.f)}{\partial t} + \frac{\partial}{\partial x_j}(\rho u_j.f) = \frac{\partial}{\partial x_j}\left[(D + D_f^t)\rho \frac{\partial f}{\partial x_j}\right] \qquad (2)$$

$$\frac{\partial(\rho.c)}{\partial t} + \frac{\partial}{\partial x_j}(\rho u_j.c) = \frac{\partial}{\partial x_j}\left[\left(\frac{\lambda}{C_p} + \frac{\mu_t}{Sc_t}\right)\frac{\partial c}{\partial x_j}\right] + \rho \dot{\omega}_c \qquad (3)$$

$$\frac{\partial(\rho.f'^2)}{\partial t} + \frac{\partial}{\partial x_j}(\rho u_j.f'^2) = \frac{\partial}{\partial x_j}\left[\left(\frac{\lambda}{C_p} + \frac{\mu_t}{Sc_t}\right)\frac{\partial f'^2}{\partial x_j}\right] - \rho\chi_t + 2\rho\left(\frac{\mu_t}{Sc_t}\right)D_f^t(\nabla.f)^2 \qquad (4)$$

Where λ/C_p is the diffusion coefficient for all species, and ν/S_{ct} is the turbulent mass diffusion coefficient, ω_c is the reaction progress source term (s^{-1}). It is retrieved from the framelet library using the expression (Eq. 1).

3.2 Steady Laminar Flamelete Approach

The steady laminar flamelet approach models, [9], the turbulent flame brush as a collection of individual steady laminar flames called diffusion flamelets. Individual diffusion flames are assumed to have the same structure as laminar flames in simple configurations and are determined by experiment or calculation. Laminar flamelet modeling of turbulent combustion is a two-step process. First, a laminar flame library is calculated by solving the governing equations for laminar flames. In the second step, the framelet profile is used as an input dataset for his CFD code. The advantage of the diffusion flame approach using detailed chemical mechanisms is that realistic chemical kinetic effects can be integrated into turbulent flames. Chemical reactions can then be preprocessed and tabulated, resulting in significant computational savings. However, the steady-state diffusion flamelet model is limited to modeling combustion due to relatively fast chemical reactions. The CFD code solves the transport equations for the average mixture fraction f and the mixture fraction variance $f^{"2}$ (Eqs.2 and 3). The average scalar loss rate can be modeled as:

$$\tilde{\chi} = 2\frac{\varepsilon}{k} f^{"2} \qquad (5)$$

where k and ε are the turbulent average kinetic energy and energy dissipation rate, respectively.
Finally, the distribution of scalars within the diffusion flame is defined as:

$$\bar{\phi} = \int_0^{\infty} \int_0^1 \phi(f,\chi) P(f,\chi) df.d\chi \qquad (6)$$

The assumption of statistical independence leads to $P(f,\chi) = P(f)P(\chi)$ where $P(f)$ is

constructed from transport equations 2 and 3.In this study uses the β-function PDF shape is given by the following function:

$$p(f)=\frac{f^{\alpha-1}(1-f)^{\beta-1}}{\int . f^{\alpha-1}(1-f)^{\beta-1}df} \quad (7)$$

where:

$$\alpha=\overline{f}\left[\frac{\overline{f}(1-\overline{f})}{\overline{f'^2}}-1\right] \quad (8)$$

and

$$\beta=(1-\overline{f})\left[\frac{\overline{f}(1-\overline{f})}{\overline{f'^2}}-1\right] \quad (9)$$

The PDF format $p(f)$ is a function only of the first two moments: the mean mixed fraction, f, and , f'^2, the variance of the mixed fraction. Species and temperature are obtained from the flamelet library (Equation 10 and Equation 11).

$$\frac{\partial T}{\partial t}=\rho\frac{\chi}{2}\frac{\partial^2 T}{\partial f^2}-\sum_{i=1}^{n}h_i\dot{\omega}_i . \quad (10)$$

$$\frac{\partial Y_i}{\partial t}=\rho\frac{\chi}{2}\frac{\partial^2 Y_i}{\partial f^2}+\dot{\omega}_i \quad (11)$$

4 Numerical Procedures

The steady-state, Reynolds Averaged Navier-Stokes equations for mass, momentum, energy, scalar transport, mean mixture fraction and mean mixture fraction variance, premixed combustion and progress variable variance are used to describe the flow physics and combustion process. The reaction rate is computed by finite rate for FGM approach and steady diffusion flamelet for the Steady Laminar Flamelet approach. The realizable k-ε turbulence model is adopted. The realizable model is used to obtain the correct spreading of a round jet. The governing equations and the associated boundary conditions are solved by a CFD code using a finite volume method. The pressure distribution is estimated by the SIMPLE technique. Calculations are performed with a uniform grid distribution. The under-relaxation factors are different for different variables varying from 0.3 to 0.7. The numerical calculations are performed on a DELL computer with CPU time of around 45 min.

5 Results and Discussions

Table 2 presents the comparison of the two models used in this study, FGM and SLF. A flamelet was produced by a counterflow flame with a strain rate of 100s^{-1}. A β-function was utilized to generate the corresponding PDF using flamelet.

The boundary conditions for the temperature and species of the problem are replaced by the boundary conditions for the mean mixture fraction, f, in this approach. In this case, the value of the mixture fraction specified in the literature, [14], f = 0.2755, was used as a boundary condition. At this value, the species distribution and temperature of the pilot gas are approximated accurately enough.

Figure 3 and Figure 4 shows the flamelet used in this study.

Table 2. PDF table creation in CFD code.

	FGM	SLF
Number of grid points in mixture fraction space	64	/
Number of grid points in reaction progress space	32	/
Initial scale dissipation (1/s)	0.01	0.01
Scale dissipation step (1/s)	1	1
Number of grid points in flamelet	/	64
Maximum number of flamelets	/	32

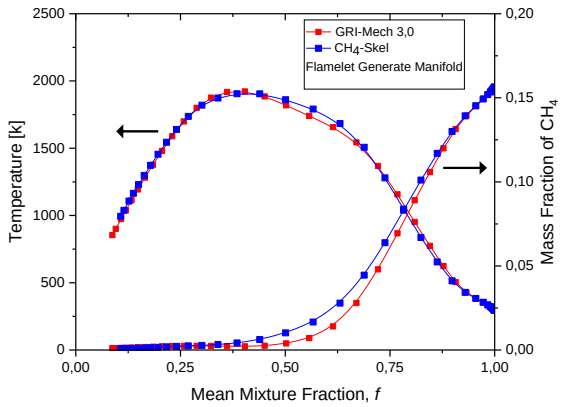

Fig. 3: Flamelet used in the simulation (RANS/FGM)

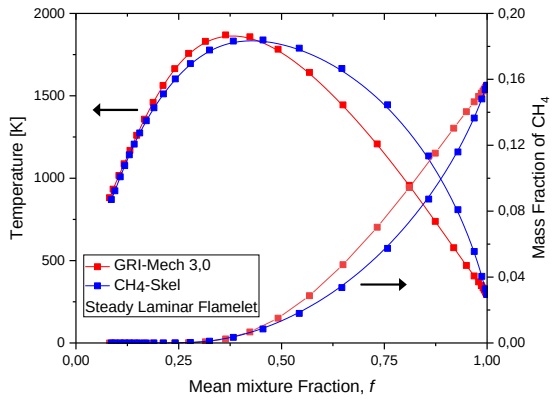

Fig. 4: Flamelet used in the simulation RANS/SLF

5.1 Flow Field and Mixing

Figure 5 and Figure 6 show a comparison between computed and experimental profiles for the mean mixture fraction in the axial direction. Along the axial direction, the computed and experimental mean mixture fraction profiles show a good agreement. The deviation of the predicted profile is slightly increasing with the axial coordinate. Examination of these two figures shows that the average mixture fraction f maintains a unit value at the outlet of the injector for the two combustion models (Partially premixed and Non-premixed) up to a distance close to x/D_{jet} =10. This reveals a delay in the mixing of the fuel (CH_4) with the oxidant (Air) at the central axis due to the round nature of the jet leaving the burner. Downstream of this station ($x/D_{jet} > 10$), the decrease begins to be felt by mixing first with the products of the pilot flame, then with the air co-current. The limit reached by the average mixture fraction corresponds to a value lower ($f = 0.1$) than its value at the injection of the pilot flame, ($f = 0.2755$). This value confirms that the air from the Co-current manages to reach (by entrainment) the central axis from the axial station ($x/D_{jet} >60$). The stoichiometric value ($f_{st} = 0.35$) of the mixing fraction as given by experimental measurements [14] is reached at the level of the axial station $x/D_{jet}=50$. In this position, part of the average flame front is supposed to be positioned ($f = f_{st}$). Figure 7 and Figure 8 show the contours of temperature distribution from the Flamelet Generated Manifold (FGM) and Steady Laminar Flamelet (SLF) combustion model descriptions with CH_4-Skel and GRI-3.0, kinetic reactions mechanisms, respectively. The visible flame extends over 35 diameters along the axial direction for the SLF combustion model and 40 diameters for the FGM combustion model, and this is in agreement with experimental data which report a visible flame length equal to about 45 diameters. In this study, the loss in accuracy, as well as the gain in run-time of the reduced description, is reported by comparing it against the full description with ISAT. The steady laminar flamelet model can simulate local chemical non-equilibrium due to the aerodynamic straining of the flame by the turbulent flow field. Species that respond quickly to this turbulence such as the OH radical can be modeled accurately (Figure 9). The OH species is representative of the important intermediate species. The impact of the reduced description on the convergence of the simulations is also reported. As shown in Figure 10, for each model, the reduced description with 16 represented species agrees well with the full description.

We can see the distribution of OH radical for the CH_4-skel mechanism reaction with the use of the Steady Laminar Flamelet method and, different from this, uses the GRI v 3.0 mechanism. By count, for the second approach ie, using the FGM method there is not a difference in the presentation of the distribution of OH. Figure 10 and Figure 11 showed different static temperature profiles on the central axis of the jet. These profiles come from calculations using two different combustion models (Partially premixed and Non-premixed) with two reaction mechanisms for the oxidation of methane in the air (GRI-Mech 3.0 and CH_4-Skel). We see the effects of two combustion models and even the two reaction mechanisms on the temperature peak and the position of this peak. In Figure 11, for the two models of combustion with the CH_4-Skel, the section relating to the temperature rise appears upstream of the experimental rate. On the other hand, in Figure 12, the section relating to the rise in temperature appears downstream of the experimental rate. Also, the decrease in temperature noted downstream of the station x/D_{jet} =50 for the two tin configurations. Table 3, illustrates this difference.

Table 3. The maximum temperature predicted by the different chemistry schemes (deviation = (prediction-measurement)/measurement)*100%).

		$T_{max.}$[K]	x/D_{jet}	Dev.[%]
Exp.	/	1960.18	45.15	/
CH_4-Skel	SLF	1841.53	37.8	-6.05
	FGM	1963.86	41.15	0.187
GRI v 3.0	SLF	1870.02	37.76	-4.6
	FGM	1905.02	38.0	-2.81

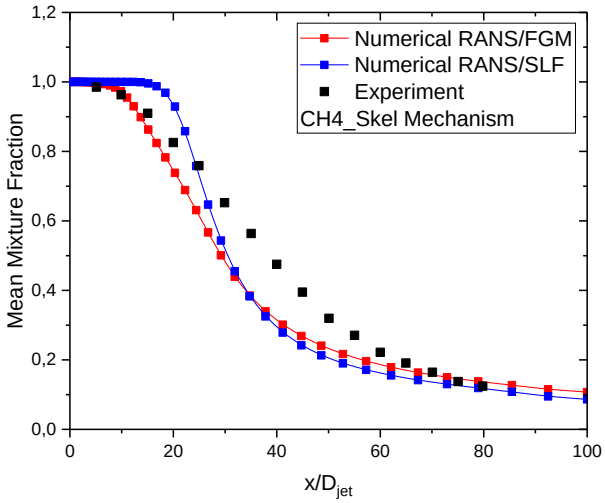

Fig. 5: Axial distribution of mean mixture fraction with CH_4-Skel Mechanism

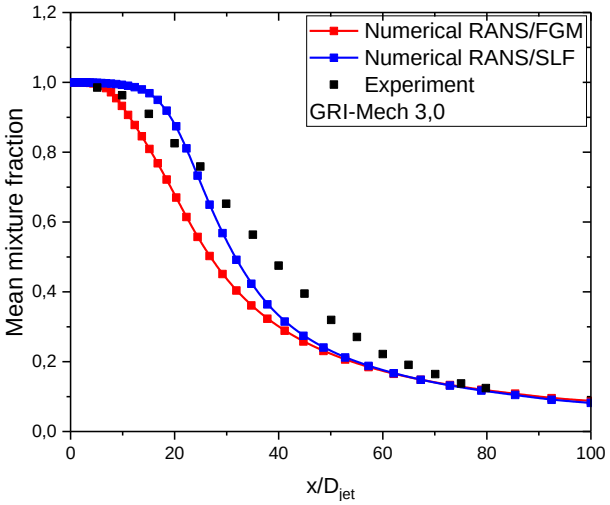

Fig. 6: Axial distribution of mean mixture fraction with GRI v 3.0 Mechanism

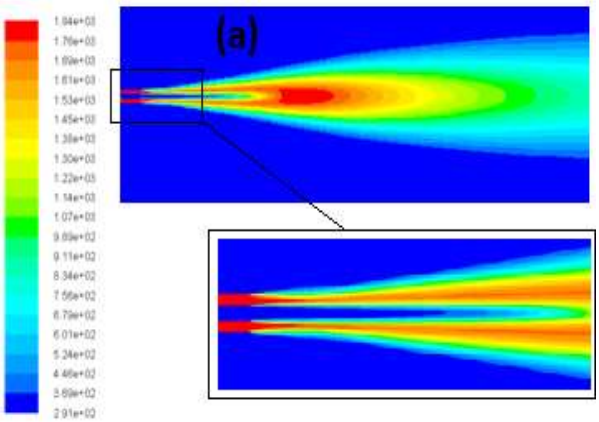

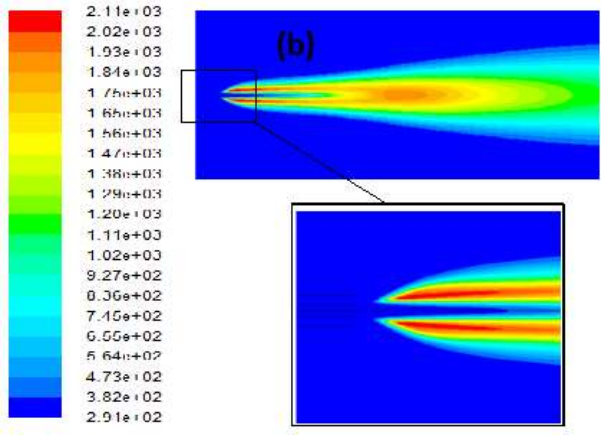

Fig. 7: Temperature distribution with CH_4-Skel mechanism: (**a**) RANS/SLF; (**b**) RANS/FGM

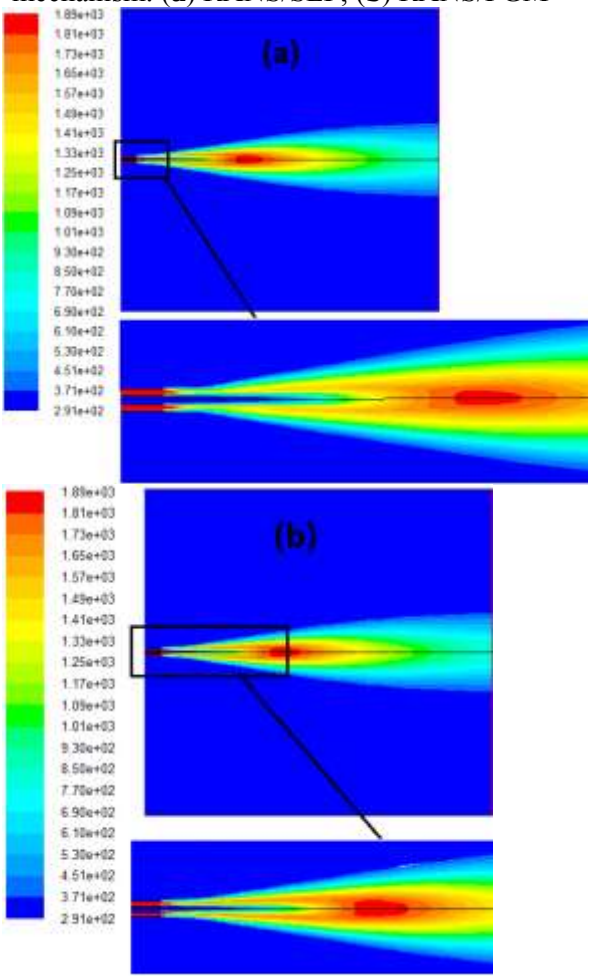

Fig. 8: Temperature distribution with GRI 3.0 mechanism: (a) RANS/SLF; (b) RANS/FGM

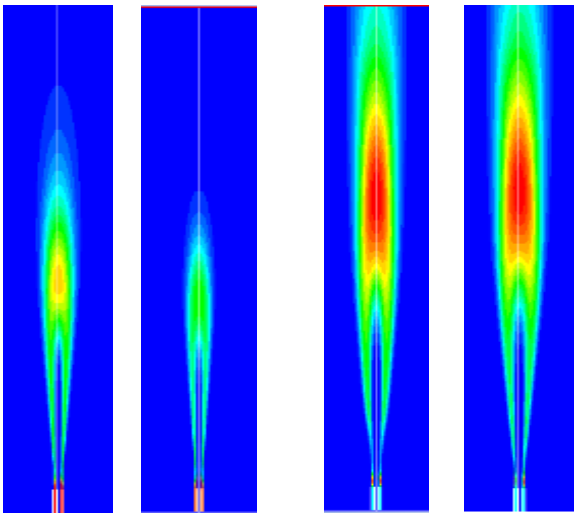

Fig. 9: Contours of mean OH mass fraction from the CH_4-Skel mechanism and GRI v 3.0 Mechanism descriptions with SLF and FGM, Methods

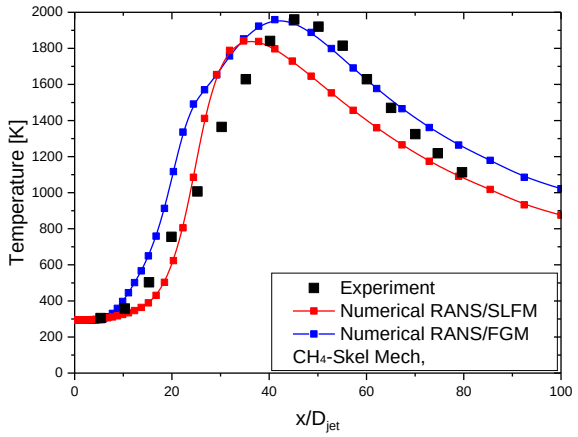

Fig. 10: Axial distribution of mean temperature: (CH_4-Skel mechanism)

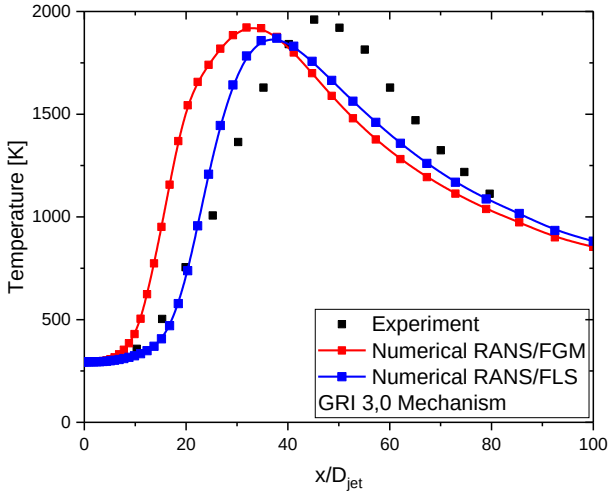

Fig. 11: Axial distribution of mean temperature: (GRI v 3.0 mechanism)

The results of the model consist of properties of the flow and the chemistry. To determine the properties of the flow, the magnitude of the velocity vector U and the turbulent kinetic energy k can be compared to the experimental data, [14].

The axial velocity plots in Figure 17 and Figure 18 show overall a very good agreement between simulation and experiment. In Figure 12, a plot of U_{axe}/U_{jet} on the x-axis is presented for partially premixed combustion with the FGM chemistry approach. At the upstream part of the domain ($x/D_{jet} < 20$), the velocity profile predicted by the models is very close to the measurements. Downstream ($20 < x/D_{jet} < 60$), the models give far too low values. Furthermore, it can be seen that the models give approximately the same values for the velocity magnitude in the entire domain.

But in Figure 13, a plot of U_{axe}/U_{jet} on the x-axis is presented for non-premixed combustion with a steady laminar flamelet chemistry approach.
At the upstream part of the domain ($x/D_{jet} > 30$), the velocity profile predicted by the models is very close to the measurements.
Downstream ($30 > x/D_{jet}$), the models give far too low values. The deviation between the models and the experiments in the prediction of axial velocity in the upstream part of the domain is caused by neglecting the velocity profile of pilot gas flowing out of the main jet inlet.

The shape of turbulent kinetic energy (Figure 14 and Figure 15) is reproduced by two models (FGM and SLF), except in the region of the fuel inlet. The high values of the turbulent kinetic energy near the fuel inlet are a consequence of the boundary conditions. The specified turbulence intensity of the fuel stream of 10% is too high. The maximum in the curve of k predicted by the simulations is too high. In addition, the experimental curve is broader than the simulations indicate. Again, it can be observed that the difference in the curves of both models is very small except for the height of the maximum.

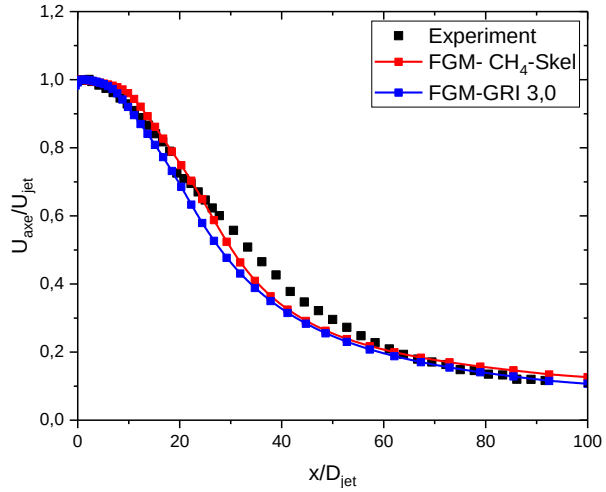

Fig. 12: Mean axial velocity (RANS/FGM)

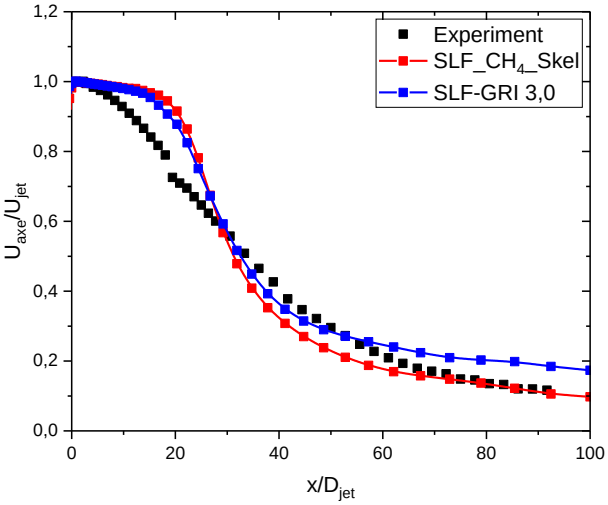

Fig. 13: Mean axial velocity (RANS/SLF)

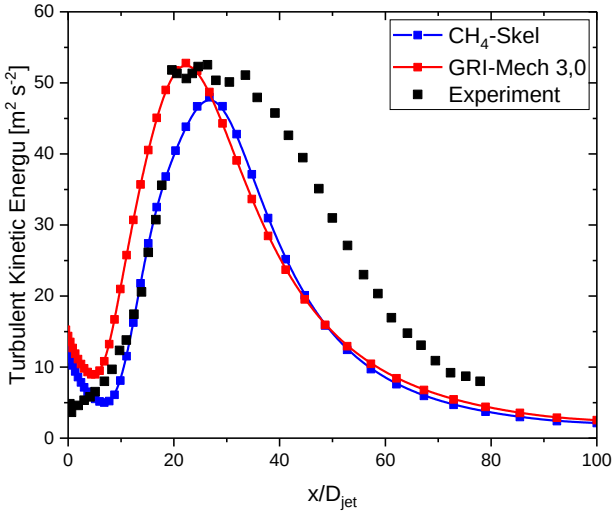

Fig. 14: Turbulent kinetic energy (RANS/FGM)

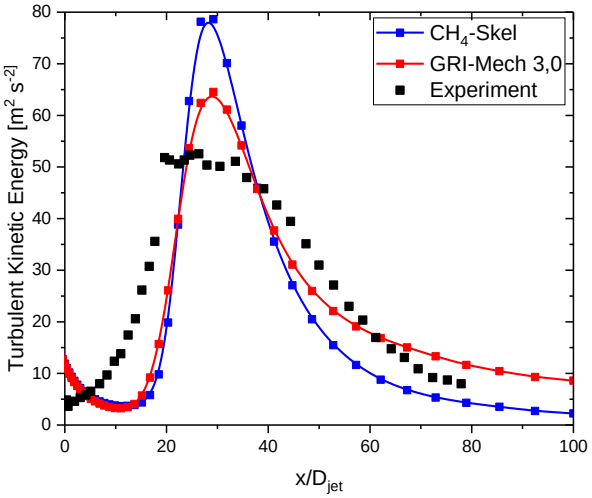

Fig. 15: Turbulent kinetic energy (RANS/SLF))

5.2 Species Prediction

Axial different species profiles (CH_4, CO_2, H_2O and O_2) along the centerline for the partially premixed combustion and non-premixed combustion as well as the FGM and SLF models are shown in Figure 16, Figure 17, Figure 18 and Figure 19, and the experiment results, [14], are also shown.

These figures show that the calculated results using FGM and SLF using the two reaction mechanisms for GRI-Mech 3.0 and CH4-Skel agree with experimental data. The accuracy of numerical predictions is good up to the height of $x/D_{jet} = 40$. We can see in Figure 9, that the temperature profile for the SLF method coincides well with the results of the experimental one in the region close to the exit of the jet ($0 < x/D_{jet} < 40$) and misrepresented in the region of $40 < x/D_{jet} < 70$.

These remarks and contrary to the notice for the second method, that is to say, the profile of the temperature with the FGM method and low in the region located between ($0 < x/D_{jet} < 40$), and indeed converges with the data from the experimental one in the region far from the exit of the jet ($40 < x/D_{jet} < 80$).

We also see the two figures which represent the evolutions of the mass fractions of the chemical species (CH_4, H_2O, CO_2 , and O_2) as for the methane fraction and well presented by the two models (SLF and FGM). It is identical when it comes to the mass fraction of oxygen. It is well represented by the two methods in the zone located between the outlet of the jet, between ($x/D_{jet} = 0$) and $x/D_{jet} = 40$), beyond this measuring station there is a difference between the numerical calculation and the experimental one.
These remarks are visibly noted for the other mass fractions for CO_2 and H_2O. Local chemical non-equilibrium caused by aerodynamic straining of the flame in the turbulent flow field can be simulated by

the steady laminar flamelet model. Species that respond quickly to this turbulent straining (such as the OH radical) can be modeled accurately.

In methane combustion, a high concentration of CO_2 will affect the flame through a direct chemical reaction of CO_2 with the fuel oxidation process. Also, as indicated from the above equilibrium calculation results, gas phase combustion mechanisms are found to play a much more important role in methane combustion modeling than in CH_4-air modeling.

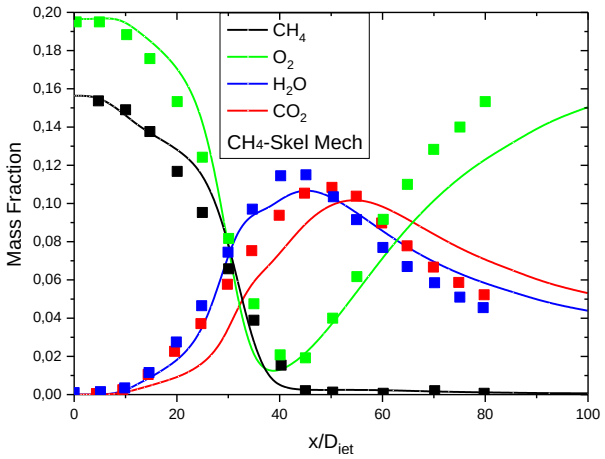

Fig. 16: Axial profiles of species mass fractions: (symbols) experiment, (lines) simulation with FGM

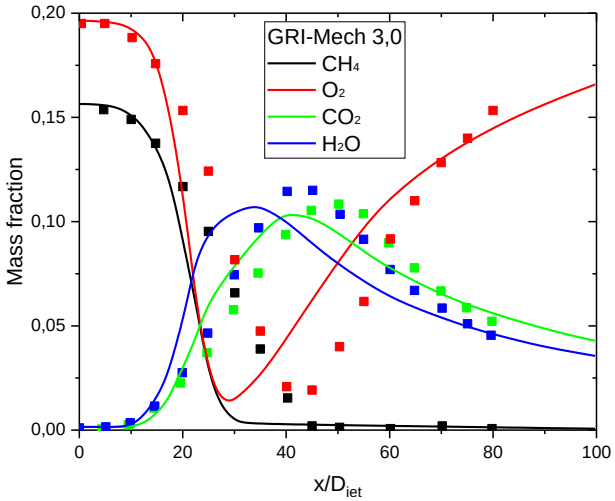

Fig. 17: Axial profiles of species mass fractions: (symbols) experiment, (lines) simulation with FGM

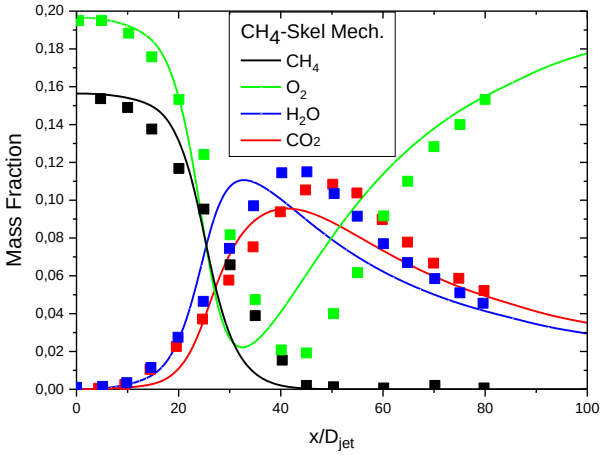

Fig. 18: Axial profiles of species mass fractions: (symbols) experiment, (lines) simulation with SLF

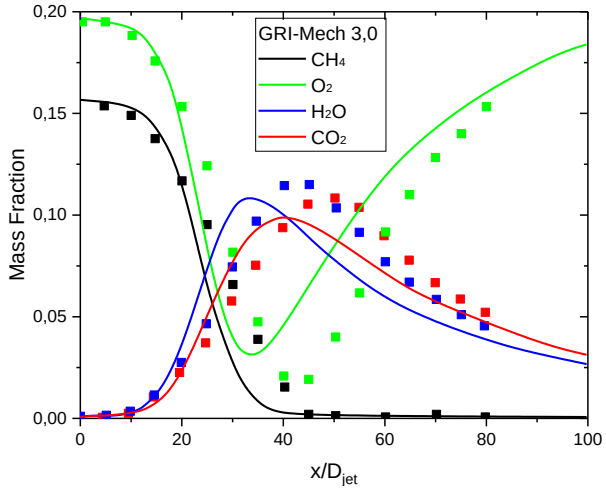

Fig. 19: Axial profiles of species mass fractions: (symbols) experiment, (lines) simulation with SLF

6 Conclusion

The goal of this work is to create and use a numerical method to simulate a diffusion flame.

The transport probability density (Pdf) model has been compared to four reacting flow test cases, including the Sandia D Flame test, in which methane and air are burned.

- A steady laminar flamelet and GRI-Mech 3.0 are used for non-premixed combustion;
- Non-premixed combustion with a Steady Laminar Flamelet and CH_4-Skel mechanism
- Partially premixed combustion with FGM and GRI-Mesh 3.0
- Partially premixed combustion with FGM and CH_4-Skel mechanism

In the context of RANS/FGM and RANS/SLF, a good agreement can be observed when comparing simulation results with experimental data

concerning temperature, velocity, chemical species, etc.

We can conclude that the use of a global kinetic mechanism such as the CH_4-Skeletal mechanism introduces an advanced variable more representative of the evolution of chemical species in the flame.

Some perspectives that could be interesting to explore for our future research can be mentioned, including:

- Start the calculations again with another reaction mechanism to create the turbulent flamelet library.
- Separate transport equations are used to determine the NOx that can be added, but their chemistry is slow and cannot be analyzed in the flamelet library.

References:

[1] Wejie Z., Suleyman K., Jinhu W., Zuo H., Jeroen V. O., Large Eddy Simulation of the Combridge/sandia stratified Flame with Flamelet-generated manifolds: Effects of Non-unity Lewis numbers and Stretch. *Combustion and Flame*, Vol. 227, pp. 106-119, 2021.

[2] Quentin C., Perrine P., Eleonore R., Bénédicte C., A fully automatic procedure for the analytical reduction of chemical kinetics mechanisms for Computational Fluid Dynamics applications, *Fuel,* Vol. 303, pp. 121-247, 2021.

[3] Laurent C., *Low-Order Modeling and High-Fidelity Simulations for the Prediction of Combustion Instabilities in Liquid-Rocket Engines and Gas Turbines*. PhD Thesis. National Polytechnic Institute of Toulouse – MeGEP Doctoral School. 6-2020.

[4] C. Laurent, G. Staffelbach, F. Nicoud, T. Poinsot, Heat-release dynamics in a doubly-transcritical LO2/LCH_4 cryogenic coaxial jet flame subjected to fuel inflow acoustic modulation, *Proceedings of the Combustion Institute,* 2020.

[5] C. Laurent, L. Esclapez, D. Maestro, G. Staffelbach, B. Cuenot, L. Selle, T. Schmitt, F. Duchaine, T. Poinsot, Flame–wall interaction effects on the flame root stabilization mechanisms of a doubly-transcritical LO_2/LCH_4 cryogenic flame, *Proceedings of the Combustion Institute,* Vol. 37, Issue 4, pp. 5147-5154, 2019.

[6] D. Laera, Stabilization mechanisms of CH_4 premixed swirled flame enriched with a non-premixed hydrogen injection, *Proceedings of the Combustion Institute*, vol. 38, nº 4, pp. 6355-6363, Janv. 2021.

[7] Gregory P. Smith, David M. Golden, Michael Frenklach, Nigel W. Moriarty, Boris Eiteneer, Mikhail Goldenberg, C. Thomas Bowman, Ronald K. Hanson, Soonho Song, William C. Gardiner, Jr., Vitali V. Lissianski, and Zhiwei Qin. GRI-Mech 3.0, [Online]. http://combustion.berkeley.edu/gri_mech/ (Accessed Date: November 10, 2023).

[8] J. A. van Oijen and L. P. H. de Goey, Modeling of Premixed Laminar Flames using Flamlet Generated Manifolds, *Combustion Science and Technology*. Vol. 161, N° 1, 2000

[9] ANSYS, Inc., *Ansys Fluent Theory Guide*, Published in the USA, 2021, [Online]. https://dl.cfdexperts.net/cfd_resources/Ansys_Documentation/Fluent/Ansys_Fluent_Theory_Guide.pdf (Accessed Date: Occtober 1, 2023).

[10] Obando V., Goussement A., Sadiki A, Parente A., Non-premixed Filtred tabulated Chemistry for LES: Evaluation on Sandia Flame D and E. *Fuels*, Vol.3, pp. 486-508, 2022.

[11] Chuanfeng Yue, Jingbo Wang , and Xiangyuan Li. Modeling of Sandia Flame D with the non-adiabatic chemistry tabulation approach: the effects of different laminar flames on NO_X prediction. *Journal of Royal Society of Chemistry*, Vol. 7,2023.

[12] Yu S., Bai X. S., Zhou B., Wang Z., Li Z. S. Aldén M., Numerical Studies of the Pilot Flame Effect on a Piloted Jet Flame. *Taylor and Francis,* Vol. 194, No. 2, pp. 351-364, 2022.

[13] He, D., Yu, Y., Kuang, Y., Wang, C. Model Comparisons of Flow and Chemical Kinetic Mechanisms for Methane–Air Combustion for Engineering Applications. *Applied Sciences.* Vol. 11, pp. 1-22, 2021.

[14] Barlow, R. S., Frank, J. H., A. N. Karpetis, and Chen, J.-Y., "Piloted Methane/Air Jet Flames: Scalar Structure and Transport Effects," *Combust. Flame* Vol. 143, N° 4, pp. 433-449 2005.

Contribution of Individual Authors to the Creation of a Scientific Article (Ghostwriting Policy)

At every stage of the present research, the authors contributed equally, from the formulation of the problem to the final findings and solutions.

Sources of Funding for Research Presented in a Scientific Article or Scientific Article Itself

No funding was received for conducting this study.

Conflict of Interest

The authors have no conflicts of interest to declare.